
Article:
Adams, C., Alborzi, E. orcid.org/0000-0002-2585-0824, Yong, X. orcid.org/0000-0003-1674-754X et al. (3 more authors) (2024) Experimental and quantum chemical investigation into the nature of jet fuel deposition on surfaces. Fuel, 358. 130101. ISSN 0016-2361

https://doi.org/10.1016/j.fuel.2023.130101

Fuel 358 (2024) 130101

Contents lists available at ScienceDirect

Fuel

journal homepage: www.elsevier.com/locate/fuel

Full length article

Experimental and quantum chemical investigation into the nature of jet fuel deposition on surfaces

Charlie Adams [a], Ehsan Alborzi [a,*], Xue Yong [b], Simon Blakey [c], Anthony J.H.M. Meijer [b], Mohamed Pourkashanian [a]

[a] Department of Mechanical Engineering, The University of Sheffield, S3 7HF, UK
[b] Department of Chemistry, The University of Sheffield, S3 7HF, UK
[c] Department of Mechanical Engineering, The University of Birmingham, B15 2TT, UK

ARTICLE INFO

Keywords:
Aviation fuel
Thermal oxidative stability
Surface deposition
Coke formation
Surface chemistry
Adsorption

ABSTRACT

Chemical analysis of undissolved deposits formed on a simulated jet fuel burner feed arm suggest a higher concentration of oxidized polar fuel species at the wall-deposit interface. To investigate the nature of their adsorption, the adsorption energies of various jet fuel species classes were calculated using plane-wave DFT methods on two oxide surfaces Fe_2O_3-(0001) and Cr_2O_3-(0001), which were chosen to represent a stainless steel surface. A mixed termination approach was chosen to encapsulate the heterogeneous nature of stainless steel surfaces. On metal-terminated Fe_2O_3 and Cr_2O_3 surfaces, the order of the absolute adsorption energies was RSO_3H > RSO_2H > RCOOH > RSH > ROH > RCOH > RH. Dissociative chemisorption was observed for all the acid species, with sulfur acids having a higher absolute adsorption energy on Cr_2O_3 but carboxylic acids having a higher adsorption energy on Fe_2O_3. On oxygen-terminated Fe_2O_3, the order of the absolute adsorption energies was RSO_2H > RSR > RSO_3H > RSH > ROH > RCOH > RCOOH > RH. On the other hand, for oxygen-terminated Cr_2O_3, the order of the absolute adsorption energies were RSO_2H > RSR > RSH > RSO_3H > RCOH > ROH > RCOOH > RH. In contrast to the metal terminated surface, acids do not chemisorb on the oxygen terminated surfaces. Instead, the sulfur acids are found to form surface hydroxyl species from the dissociation of the acidic -OH group. The reactivity of the surfaces followed the general pattern: metal terminated-Fe_2O_3 > metal-terminated Cr_2O_3, oxygen-terminated Fe_2O_3 ≈ Cr_2O_3. Overall, a combination of experimental and quantum chemical techniques confirmed the theory that sulfur acids are the initial species to deposit on stainless steel.

1. Introduction

Irrespective of the source of an aviation fuel, one of the crucial technical suitability considerations for the utilization of fuel is its resistance to thermal oxidative degradation. Thermal oxidative stability is a regulated property, since jet fuel has a secondary function as a cooling fluid, prior to the combustion chamber [1]. Thermal oxidative degradation will become increasingly important in the future as more thermally efficient jet engines are brought into service, resulting in larger heat loads on the bulk fuel [2]. The development of a robust theoretical framework for thermal oxidative degradation through an understanding of the molecular interactions between fuel species and components will enhance the prediction of the growth of surface carbonaceous deposits in aero-engine fuel systems [3]. However, this requires a comprehensive quantitative/qualitative analysis of a large number of chemical species interacting with the surface during fuel thermal degradation. The complex chemical composition of aviation fuel means that efforts to understand the mechanisms behind deposition, to date, have involved a combination of theoretical studies and experimental work carried out under simplified conditions [3–5].

Experimentally, jet fuel system simulators such as the Aviation Fuel Thermal Stability Test Unit (AFTSTU) are capable of assessing fuel thermal degradation in service conditions [4]. The AFTSTU rig replicates conditions in a range of current and future aero-engines, ensuring that the fuel arrives at the simulated burner feed arm in a condition which is representative of a system in terms of fluid flow, thermal exposure, surface chemistry, etc.

The term thermal oxidative stability refers to the ability of an aviation fuel to withstand chemical changes caused by reactions with oxygen dissolved in the liquid phase [6]. Thermal oxidative degradation can be divided into two key processes: (i) autoxidation of

* Corresponding author.
E-mail address: e.alborzi@sheffield.ac.uk (E. Alborzi).

https://doi.org/10.1016/j.fuel.2023.130101
Received 30 April 2023; Received in revised form 13 August 2023; Accepted 12 October 2023
Available online 2 November 2023

the fuel, (ii) subsequent formation of insoluble species leading to deposits. The autoxidation of the bulk fuel produces several oxidized fuel species including acids (RC(=O)OH), alcohols (ROH) and carbonyl compounds (RCHO) [3]. Minor heteroatomic species (such as nitrogen and sulfur-containing species) are also oxidized via reactions with hydroperoxides (ROOH). Of these heteroatomic species, indigenous sulfur compounds are known to be strongly deleterious to fuel thermal stability. In particular, thiols [7–9], successively react with hydroperoxides to form sulfenic (RSOH), sulfinic (RS(=O)OH) and sulfonic (RS(=O)2H) acids [10,11].

The oxidized species RCHO, ROH, RC(=O)OH along with sulfur-containing species RSOH, RS(=O)OH, $RS(=O)_2OH$ formed through the autoxidation process are believed to take part in agglomeration processes. These oxidized species then eventually bind to heated surfaces, forming carbonaceous deposits [12]. This binding process, known as thermal oxidative deposition/metal catalytic coking, occurs in the range of 150-350 °C [13]. However, it is yet unclear which chemical mechanisms or fuel species are involved in different stages of deposition. It has been reported that deposits generated in aviation fuel systems are 'varnish-like' or 'lacquer-like', as they are difficult to remove mechanically [14,15]. The high temperatures (500 −800 °C) required to completely remove deposits using thermal gravimetric analysis (TGA) and carbon burn-off methods suggest that deposits are chemically bonded to the heated surfaces [4,16].

Direct analysis of deposits from lab scale tests, and subsequent characterization of constituent elements and functional groups has collectively helped to propose potential mechanisms of deposition. Stainless steel (SS) 316 is one of the most common materials found in the fuel lines of an aero-engine. Therefore, it has received extensive attention as a substrate for deposition [16–18]. For example, Ervin et al. used X-ray Photoelectron Spectroscopy (XPS) to confirm the higher concentration of S-O bonds at early stages of deposit growth [16]. Moreover, atomic emission spectroscopy (AES) measurements carried out by Kauffman et al. demonstrated a higher concentration of sulfur and oxygen at the deposit-surface boundary [17]. The presence of S-O bonds allowed both papers to postulate that organic sulfur acids formed from autoxidation of reactive sulfur play a key role at the early stage of deposition. Complementary to this, Venkataraman et al. reported that deposits show high levels of oxygen-containing functional groups together with the presence of carboxyl moieties via thermogravimetric analysis-mass spectroscopy (TGA-MS). The latter was confirmed by XPS [19]. In addition, sulfonic and carboxylic acids have been shown to react with SS316L surfaces. However, the mode of interaction in this case has not been fully elucidated [20]. In contrast to the involvement of oxidized fuel species in wall attachment, Beaver et al. proposed that aryl thiols are important for deposit formation [12]. Mohan et al. also theorize that thiols and disulfides directly form metal sulfides on a variety of SS surfaces [21]. Finally, metal sulfides have also been shown to form at higher pyrolytic temperatures on stainless steel by several researchers [19,22].

From a theoretical point of view, density functional theory (DFT) has emerged as an increasingly important tool to understand thermal oxidative degradation. DFT allows proposed reaction pathways to be evaluated in terms of calculated thermodynamic and kinetic parameters. Publicly available DFT studies pertinent to jet fuel thermal stability have mainly focused on liquid phase chemistry in bulk fuel [10,23,24]. Within recent years, plane-wave pseudopotential methods implemented in DFT have become useful tools for investigating surface chemistry [25–27]. Within the scope of fuels, DFT calculations using the Vienna Ab Initio Package (VASP) has been applied to explore the reactivity of surfactants on stainless steel surfaces in automotive engines [25]. Additionally, a recent study has employed DFT calculations to study the adsorption of bio-fuel species on stainless steel [28]. To our knowledge, no DFT studies have investigated the reaction of thermally oxidized conventional jet fuel species occurring at the surface-fuel interface, i.e. reactions occurring between the fuel and pipe walls.

Morphological analysis of fuel deposits reveals that the thermally stressed fuels initially form a thin film of deposit on SS. This film then manifests itself as particle growth at specific sites [16]. Kauffman et al. postulated that site-specific growth could occur at grain boundaries on stainless steel [17]. Stainless steel primarily is passivated by a chromium layer. However, grain boundaries reveal local chromium depleted zones which exposes iron-based oxides [29]. Furthermore, steel passivation layers tend to contain both chromium and iron oxides of differing phases. Thus, local oxides could interact with deposits in different ways. Unfortunately, because of the high molecular weight and amorphous nature of jet fuel deposits, direct analysis of deposits can only provide limited information about their structure. Furthermore, it is difficult to study deposit growth *in situ*, because of the difficulty of sampling and the rapidity of deposit layering at the nano-scale.

The aim of this article is to identify which indigenous/oxidized fuel species have the greatest propensity to adsorb on clean stainless-steel surfaces using DFT calculations. A complication in this is the fact that SS is heterogenous in structure, whereas predictive numerical mechanisms require the wall to be treated as a mono-component surface with uniform reactive properties [3]. Thus, the adsorption energies of fuel species for two main surface oxides, hematite and chromia, was compared. Two main classes of species and their main autoxidation products were assessed. Firstly, bulk hydrocarbons (RH) which will be represented by a simple alkane as the most common species in conventional and alternative fuels [29,30]. The bulk hydrocarbon autoxidation products investigated will be carbonyl (RCHO), alcohol (ROH) and carboxylic acid (RC(=O)OH) species. Secondly, sulfur species represented by a thiol (RSH) and sulfide (RSR), which are found in conventional fuels. The main products of thiol (RSH) autoxidation, sulfinic (RS(=O)OH) and sulfonic ($RS(=O)_2OH$) will also be assessed. The DFT results were compared with the elemental analysis of carbonaceous deposits at the early stage of deposition, obtained from the wetted surface of a simulated burner feed arm, as part of Aviation Fuel Thermal Stability Test Unit (AFTSTU).

1.1. Results from the aviation fuel thermal stability (AFTSTU) rig from previous results

Fig. 1 presents the distribution of the elements in an area covering small parts of stainless steel and deposit layer generated in the AFTSTU rig. These results suggest that Fe atoms are more concentrated in stainless steel and reduce significantly throughout deposit. On the other hand, the Cr component is closer to the steel wall surface, indicating the passivating layer [31]. With the exception of the early stage of deposit, close to the surface, C atoms are evenly distributed throughout the different stages of deposition. This suggests that deposition at later stages is dominated by C-C interactions. O atoms are more concentrated at the early and later stages of deposit structure; sulfur atoms show more contribution at early stage and become patchy throughout deposit. Interestingly, the concentration of oxygen and sulfur is located at similar spots at the wall-deposit interface, suggesting the involvement of an oxidized sulfur species. The change of the pixel density associated with each element in the deposit structure is displayed in Fig. 1. This analysis reinforces the fact that the sulfur and oxygen density is closely related at the wall-deposit interact.

As noted above, the late stage development of the deposit is outside the scope of this work, but our results are consistent with a deposition layer composed largely of polar species. In this work we focus on the origins of the fuel–wall interactions at the early stage using DFT calculations (see Fig. 2).

2. Methods

2.1. Surface model

Stainless steel is heterogeneous in structure [17,29]. Therefore, α-Cr_2O_3 and α-Fe_2O_3 oxides were chosen as the surfaces to represent stainless steel in this study. Fe_2O_3 and Cr_2O_3 are isostructural

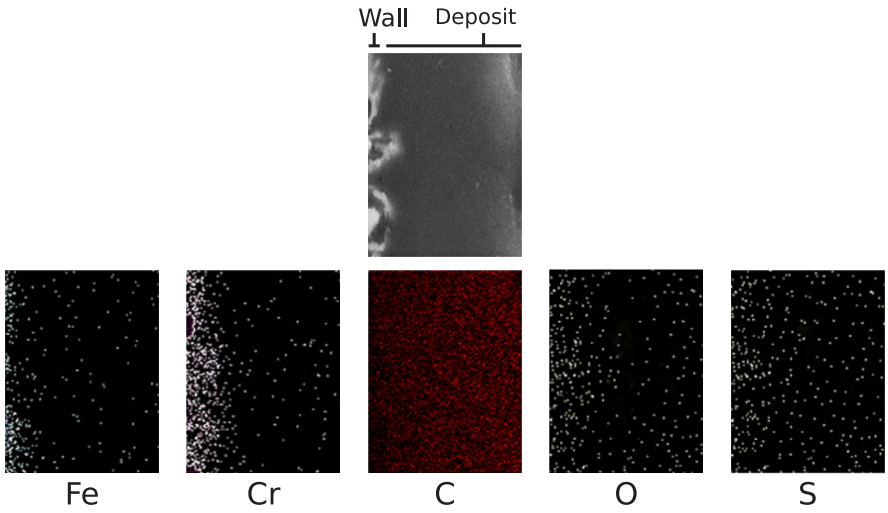

Fig. 1. Map of constituent elements detected via EDX of deposit generated in an AFTSTU burner feed-arm corresponding to an arbitrary point, the corresponding SEM image of the area is shown at the top.

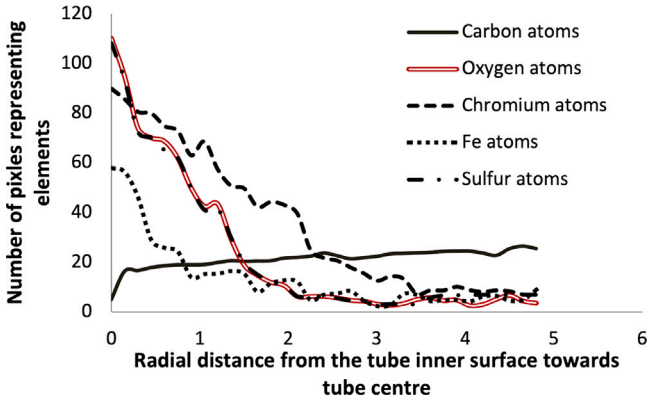

Fig. 2. Pixel analysis of the elemental constituents moving through the deposit layer presented in Fig. 1.

species. Both are found in corundum type structures. The (0001) lattice planes were used for both given that they are common in steel [32]. Additionally, surface energy calculations have shown that the (0001) plane has the highest stability for both surfaces [33,34]. Both metal and oxygen-terminated surfaces will be studied, in-line with recent computational work exploring the reactivity of stainless steel [27]. Nevertheless, we acknowledge that a metal-terminated surface has frequently been shown to have the highest stability for pure α-Cr_2O_3 and α-Fe_2O_3 [32,35,36].

To construct the surfaces, bulk hexagonal unit cells and ions were relaxed. Two surfaces with four/six layers were built based on the optimized bulk cells. A 20 Å vacuum was added above the surface to avoid periodic image interactions. The bottom two layers were fixed during structure optimization. Each bulk and surface unit cell consisted of a slab roughly 12 Å thick which was built from four stoichiometric units. All structures were assigned their most stable magnetic ordering at standard conditions. Thus, Fe_2O_3 exhibits ferromagnetic coupling within each Fe bilayer and anti-ferromagnetic coupling between neighboring bilayers along the (0001) direction [37]. In contrast, Cr_2O_3 exhibits anti-ferromagnetic coupling within the bilayers and ferromagnetic coupling between adjacent Cr layers [38].

All surface models were prepared using the pymatgen python package [39,40]. The molecules were placed 1.6 Å above the surface aligned with functional groups 2 potential sites corresponding to metal and oxygen top-sites. These sites were selected out of all possible adsorption sites (Fig. 3) likely to be important. For each top-site, the slab and adsorbate geometries were optimized to a minimum. Each calculation corresponds to a high-coverage scenario, because a (1 × 1) unit cell was chosen. A high coverage scenario was chosen, because of the number of species, configurations and surfaces that were tested, given the available resources. Additionally, a high-coverage scenario allows the lateral interaction between adjacent polar species on heated surfaces.

2.2. Computational details

All density functional theory calculations were performed using the Vienna Ab Initio Simulation Package (VASP), version 5.4.4 [41–43]. The generalized gradient approximation (GGA) was used with the optimized Perdew, Burke, and Enzerhof functional (OptPBE) [44]. OptPBE improves the accuracy of the original PBE functional by adding a non-local correlation energy using a model response functional which uses electron densities [34]. Addition of this vdW-DF allows long-range dispersion interactions to be accounted for, where localized GGA functionals are often inaccurate [45]. Inclusion of long-range interactions makes the OptPBE functional particularly suitable for surface interactions. Our own testing of the OptPBE, PBE, and the meta-GGA SCAN functionals demonstrate that PBE under-binds for chemisorbed and physisorbed fuel species on both oxides. These results are presented in Table 1 and discussed in Section 2.3. To describe the highly correlated 3d-electrons in α-Fe_2O_3 and α-Cr_2O_3 the rotationally invariant approach proposed by Dudarev et al. was chosen as the DFT +U method [46]. For Fe the U-J parameter was 4.0 eV, which gave a band gap of 2.07 eV and magnetic moment of 4.14 μ_B, close to the experimental band gap of 2.4 eV and measured magnetic moment range of 3.32 – 4.20 μ_B [47]. For Cr a U-J parameter of 4.0 eV gave a band gap of 3.22 eV and a magnetic moment of 2.91 μ_B, compared to the experimental values of 3.4 eV and 3.8 μ_B band gap and magnetic moment, respectively [20]. The core electrons were replaced by projector augmented wave (PAW) potentials [48,49]. The wave function of the valence electrons was cut-off at 600 eV [50,51]. For both α-Fe_2O_3 and α-Cr_2O_3, a Monkhorst–Pack 7 × 7 × 1 k-point grid was in used the surface calculations, where a dipole correction was added to account for the asymmetry of the slabs. For the bulk calculations a 7 × 7 × 7 Monkhorst–Pack k-point grid was employed. Bader charge analysis was performed by the code written by the Henkelman group [52–55].

The adsorption energies, E_{ads}, were calculated as follows:

$$E_{ads} = \left(E_{sys} - E_{slab} - N_{mol} \times E_{mol}\right) / N_{mol} \quad (1)$$

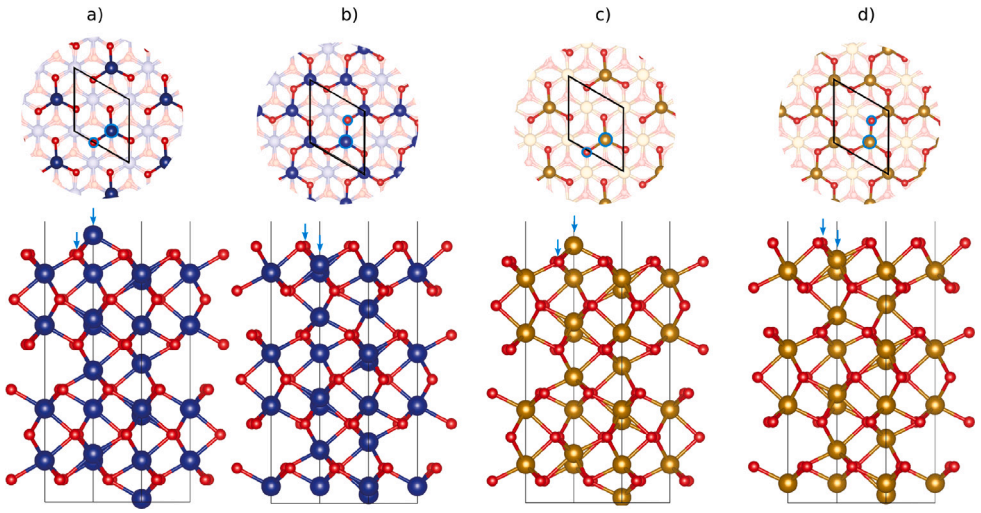

Fig. 3. Surfaces used in this study, blue atoms represent chromium, brown atoms represent iron and red atoms represent oxygen. Panel (a) correspond to metal terminated Cr_2O_3 (Cr-O_3-Cr). Panel (b) corresponds to oxygen terminated Cr_2O_3 (O_3-Cr-Cr). Panel (c) metal terminated Fe_2O_3 (Fe-O_3-Fe). Panel (d) oxygen terminated Fe_2O_3 (O_3-Fe-Fe). Green arrows and circles indicate the chosen adsorption sites for this study, at the top site metal and oxygen for each respective surface. (For interpretation of the references to color in this figure legend, the reader is referred to the web version of this article.)

Table 1
Calculated adsorbtion energies eV of ethane sulfonic acid on metal terminated Fe_2O_3 and Cr_2O_3 using different functionals.

	Fe_2O_3		Cr_2O_3	
	Metal top-site	Oxygen top-site	Metal top-site	Oxygen top-site
PBE	−0.31	−1.55	−0.36	−1.73
OptPBE	−1.26	−2.48	−1.01	−2.56
SCAN	−0.90	−2.11	−0.93	−2.76

where E_{sys} is the energy associated with the optimized structure of the adsorbate on the slab, E_{slab} is the energy associated with the clean slab, and E_{mol} is the energy of the adsorbate calculated in a large $20 \times 20 \times 20$Å box. N_{mol} is the number of adsorbates per unit cell [25].

We also consider the energy contribution of lateral interactions below. They were calculated using:

$$E_{lateral} = E_{molsurf} - E_{mol}, \tag{2}$$

where $E_{molsurf}$ is the energy of the frozen adsorbate, obtained from the geometry of the fully-relaxed structure on the slab after the slab is removed (as described in the surface model section).

2.3. Justification for using the OptPBE functional

Due to the difficulty in obtaining reliable experimental data for adsorbtion energies, often the comparison of different functionals is used to justify the choice of functional [27]. As a result, we compared OptPBE with PBE (GGA) and the SCAN (meta-GGA) functional. The cutoff energy used for these tests was 450 eV and a gamma centered 4x4x2 k-point grid was used. The SCAN functional has been shown to give accurate results for covalent and long-range systems for both solid state and molecular systems, often improving on the accuracy of more expensive hybrid functionals [56]. The ethane sulfonic acid adsorbate was selected for testing each functional since it was expected that this group would exhibit the both strong chemisorption and long-range interactions. The adsorption energies for each functional are presented in Table 1. It is clear that PBE underbinds at the chemisorption site (oxygen top-site), and the physisorbtion site (metal top-site). By contrast both the SCAN and OptPBE functional gave similar results at each site. The OptPBE functional was chosen for this study because of its lower overall computational cost.

2.4. Choice of alkyl chain-length

Since this study is primarily concerned with the reactivity of the functional groups of various fuel species with stainless steel, a short ethane carbon chain was used rather than more typical jet fuel species. Indeed, the average chain length of a jet fuel hydrocarbon is C_{12} [6]. This was computationally too costly, given the available resources, due to the large gap which would be required between the slabs. Thus, a C_2 chain was selected instead, to minimize the computational cost. Additionally, a shorter chain reduces the number of possible conformations of the alkyl tail. Nevertheless, in general, a longer alkyl tail increases adsorption energy due to adjacent VdW packing (see Figure 14 in the SI for the effects of tail length), observed in recent work on high-coverage surfactant adsorption on SS [25]. A shorter tail reduces the complexity of the calculations without sacrificing insight into different fuel species.

3. Results and discussion

3.1. Computational results

In this section, DFT-calculated adsorption energies for oxidized and indigenous fuel species on Fe_2O_3 and Cr_2O_3 are presented and discussed. Geometry optimization of the clean M-terminated (metal terminated) surfaces led to the inward relaxation of the top metal sites, leading to a contraction in the interlayer metal top-layer and oxygen layer. For clean O-terminated (oxygen terminated) surfaces, geometry optimization also led to an inward relaxation of the top-site oxygens. The optimized clean surface geometries are present in the SI Figure 3. The surface energy for the M-terminated Fe_2O_3 and Cr_2O_3 surfaces were $1.52\,J\,m^{-2}$ and $2.03\,J\,m^{-2}$ respectively, matching well with previous data [57,58]. The O-terminated surfaces had higher surface energies $3.09\,J\,m^{-2}$ and $3.69\,J\,m^{-2}$ for Fe_2O_3 and Cr_2O_3, owing to the large dipole induced by the non-stoichiometric surface.

The DFT results will be related to the AFTSTU experimental work and existing observations for fuel systems [12,16,17,19]. Fig. 4 shows the adsorption energies for each of the surfaces and for the given fuel species. Tables 4 and 3 in the SI give details of the adsorption energies, and tabulate the contribution of lateral VdW interactions to the total adsorption energies. Section 10 contains the geometries of all the adsorbates and surfaces tested.

Our VASP calculations show that sulfur acids play an important role in binding to the heated surface in the deposition process as

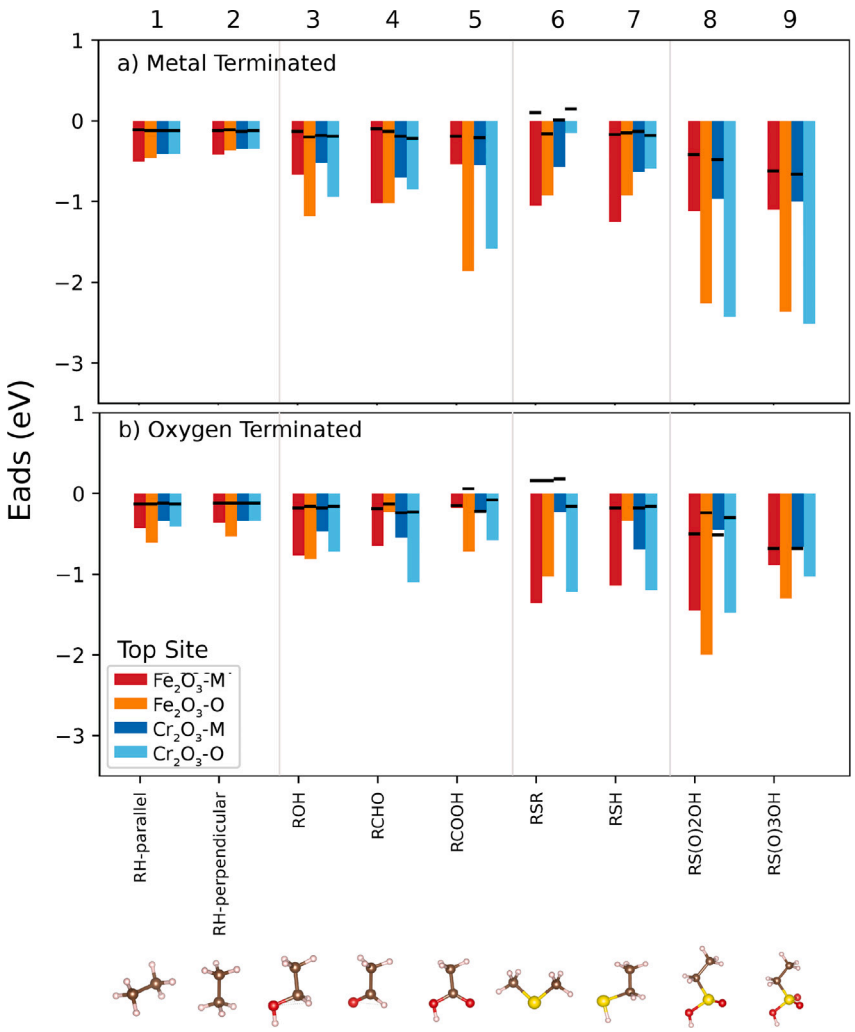

Fig. 4. Adsorption energies calculated using OptPBE for the high coverage metal-terminated and oxygen-terminated surfaces. The key indicates whether the geometry relaxation was initiated the metal-top (-M) or oxygen-top (-O) sites. The adsorbates displayed at the bottom are the initial configurations which are set to relax on each surface. The black bars indicate the VdW contributions towards the total adsorption energy.

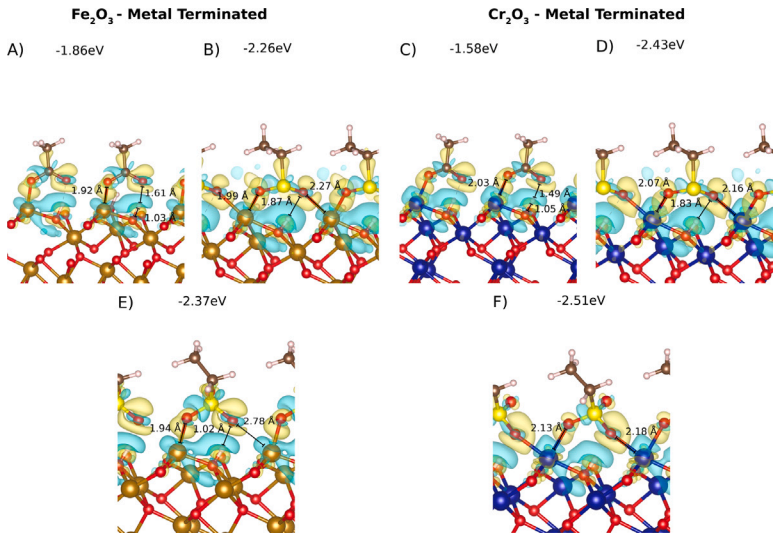

Fig. 5. Chemisorbed geometries in our tests including charge density difference plots,.

proposed by previous researchers [16,17,59]. In particular, the detection of higher concentrations of O and S at the wall/deposit interface of the AFTSTU burner feed arm is consistent with the accumulation of acidic sulfur species. However, the adsorption energies show that each oxidized sulfur species exhibits individual behavior on the surface depending on the surface termination and the specific oxide under consideration.

Firstly, only M-terminated surfaces lead to dissociative chemisorption adsorption of oxidized sulfur species to the wall, where the adsorption of sulfur acids is presented in panels in **B**, **D**, **E** and **F** Fig. 5. This adsorbtion is characterized by metal ester bond formation (S/C-O-M), and will involve the dissociation of the acid O-H to a top-site oxygen, and a C-O-M bond forming with a top-site methal. Hereby, dissociative adsorption of sulfur acids on Cr_2O_3 is more favorable than on Fe_2O_3. This contradicts the assertion by previous researchers that Cr-depleted zones could provide a favorable site for deposition [17]. Nevertheless, the deposition process in conventional fuels is almost always characterized by an induction period, where components like thiols are oxidized [7]. Therefore, the formation of sulfur acids before the start of deposition corroborates well with previous observations.

All acids tested formed metal ester bonds via the top site metal on the M-terminated surfaces (Fig. 5). Ethanoic acids were adsorbed as monodentate metal-ester structures on both surfaces (Fig. 5**A** and **C**). However, all the sulfur acids (with the exception of sulfinic acid on Fe_2O_3) were adsorbed as bridging bidentate metal-esters formed on adjacent M top-sites. On O-terminated surfaces, acid −OH groups tended interact with the top O layer (Figures 16 and 20 in the SI). In general, acids on O-terminated Fe_2O_3 had the highest absolute adsorption energies compared to O-terminated Cr_2O_3. Interestingly, sulfur acids dissociated on O-terminated Fe_2O_3 forming surface −OH groups.

In contrast to the sulfur acids favorable binding on M-terminated Cr_2O_3, non-oxidized sulfur compounds tended to have a higher absolute adsorption energy on M-terminated Fe_2O_3. Thiols tended to have a higher absolute adsorption energy than sulfides on both M-terminated surfaces, where poor packing abilities of the sulfide methyl groups led to repulsive VdW interactions reducing the total adsorption energy (Figure 17 in the SI). Both non-oxidized sulfur compounds are stabilized by favorable sulfur lone-pair M-topsite interactions. On O-terminated surfaces, in general sulfides had higher absolute adsorption energies. In fact, on the O-terminated surfaces, at the M-topsites, sulfides form sulfoxides upon adsorption. Thiol adsorption is characterized by favorable −SH O-topsite interactions. However, on O-terminated Fe_2O_3 the adsorption of thiol also leads to the formation of surface −OH groups. In contrast with Beaver et al.'s SMORS proposal, no aryl sulfide formation was observed on any of our oxides tested [12]. Nevertheless, stable physisorbed structures formed on both surface terminations could cover further adsorption at these sites, suggested by previous researchers [60].

Potential alternative future fuels like power-to-liquid fuels will contain no sulfur. Instead, the major products of thermal oxidative stressing will be oxygenated species [28]. For the oxygenated species on the M-terminated surfaces, Fe_2O_3 provides the highest absolute adsorption energies. Nevertheless, both M-terminated surfaces follow a similar adsorption trend of RC(=O)OH > RCOH ~ RCHO > RH. This result mirrors similar work on biofuel molecules on Cr_2O_3 M-terminated surfaces [28]. In general, physisorbed geometries of the oxygenated species are stabilized by O-M interactions, where stable dative bonds are formed (Figure 15). These dative bonds are characterized by the interaction between the oxygen lone-pair and the cationic top-site metal. For the O-terminated surfaces, Fe_2O_3 tends to provide the highest stability for oxygenated species with the exception of RCHO on O-terminated Cr_2O_3.

On both surfaces and terminations, surface-adsorbate adsorption of the oxygenated compounds is stabilized by high levels of VdW lateral interactions. Because high levels of oxygenated species has previously been correlated with high levels of deposit [61], an increased concentration of oxygenated species at the wall will increase the stability of oxygenated species simultaneously adsorbed at the wall. Additionally, despite the fact that no chemisorption was found for the oxygenated species we tested, formation of meta-stable physisorbed structures would still increase the residence time of these species in the fuel system. It has been shown that increased residence time results in the production of larger amounts of deposit because of the ability of species to undergo further autoxidation and agglomeration reactions [62]. Looking into the future, fuels will contain lower levels of sulfur compounds but conversely be more susceptible to form autoxidation products like carboxylic acids, as SAF fuels become more popular. Existing numerical mechanisms tend to model deposition as a single **Deposit Precursor→Deposit** step [2,3,63]. However, our AFTSTU experimental data shows a changing chemical composition moving away from the SS wall (Fig. 1). In addition, our VASP results suggest that once adsorbed, fuel species would block any further reaction with the surface. Therefore, after initial adsorption, if the surface is fully covered, further deposition will be no longer characterized by metal–fuel interactions, but by carbon–carbon interactions. Our previous work et al. has proposed a two-stage deposition mechanism based on this phenomenon [64]. However in Ref. [64], the thermochemical and kinetic parameters were correlated from experiments using a conventional fuel with a specific fuel chemistry. Recent work has shown that quantum chemistry calculations integrated into predictive numerical mechanisms have the potential to create more generalized mechanisms, applicable to multiple fuel chemistries [65]. Our study has demonstrated that DFT calculations can begin to explain the behavior of different fuel types. A larger study of a variety of compounds and surface types, including structural variations of adsorbates, would provide the opportunity to construct a predictive deposition mechanism using these techniques. Indeed, high throughput surface calculations could offer a way of constructing a larger data-set for the task of constructing a predictive numerical mechanism for future fuels [66].

3.2. Conclusions

The adsorption of representative jet fuel species on representative stainless steel oxides (hematite and chromia) was studied using plane-wave DFT calculations. In addition, the AFTSTU rig was employed to study chemical composition throughout the deposit–wall structure. Results from the AFTSTU rig indicate higher levels of sulfur and oxygen at the deposit–wall interface. DFT calculated adsorption energies show that sulfur acids and carboxylic acids are able to chemisorb on metal-terminated Fe_2O_3 and Cr_2O_3. Interestingly, sulfur acids show a larger binding strength for metal-terminated Cr_2O_3, whereas carboxylic acids show greater stability on metal-terminated Fe_2O_3. Future sustainable aviation fuels (SAF) are expected to have a lower sulfur content. Therefore, higher levels of carboxylic acids are expected to be formed from autoxidation. Thus, the deposition on steel is expected to be slower and found at Cr-depleted zones.

Unoxidized sulfur compounds showed a lower reactivity towards the surface. However, thiols and sulfides were still able to form stable physisorbed structures, particularly on Fe_2O_3. The bulk fuel component, represented by ethane, was inert towards both surfaces as expected. Oxidized bulk fuel components, ethanol and ethanal, were able to form stable physisorbed structures via dative bonds. Since the aim of the work was to guide the future formation of predictive deposition models, the generalizability of heterogeneous stainless steel was also explored within the DFT calculations. In general, metal-terminated surfaces led to a larger binding energy. In addition, binding energies were larger for both terminations of the Fe_2O_3 surface. However, many exceptions were found to this observation, notably for the chemisorption of sulfur acids on Cr_2O_3.

Our experimental results combined with surface DFT calculations show that both techniques can be used successfully in combination

to explore complex deposition phenomena in fuels. Future fuels will have a lower proportion of heteroatomic components. However, higher temperature demands on fuels, and the expectation that conventional fuel will be continually used as a blend, means that thermal oxidative stability will still be important. In particular, our study has shown the formation of carboxylic acids from fuel autoxidation will remain a problem as long as hydrocarbon fuels are used.

CRediT authorship contribution statement

Charlie Adams: Writing – review & editing, Writing – original draft, Visualization, Methodology, Investigation, Data curation, Conceptualization. **Ehsan Alborzi:** Writing – review & editing, Supervision, Methodology, Investigation, Formal analysis, Conceptualization. **Xue Yong:** Writing – review & editing, Supervision, Conceptualization. **Simon Blakey:** Writing – review & editing, Funding acquisition, Conceptualization. **Anthony J.H.M. Meijer:** Writing – review & editing, Supervision, Methodology, Investigation. **Mohamed Pourkashanian:** Writing – review & editing, Conceptualization.

Declaration of competing interest

The authors declare that they have no known competing financial interests or personal relationships that could have appeared to influence the work reported in this paper.

Data availability

No data was used for the research described in the article.

Acknowledgments

All the calculations were performed on the University of Sheffield's Bessemer, Sharc and Sol HPC clusters. The work was partly funded by the University of Sheffield, Department of Mechanical Engineering, PhD scholarship scheme, UK and the Fuel INjector Coking and Autoxidation Prediction (FINCAP) project, UK under the Grant agreement ID: 755606.

Appendix A. Supplementary data

Supplementary material related to this article can be found online at https://doi.org/10.1016/j.fuel.2023.130101.

References

[1] D1655 A. Standard specification for aviation turbine fuels. Annual Book of Standards, ASTM International West Conshohocken, PA; 2010.
[2] Jia T, Pan L, Gong S, Xie J, Wang X, Fang Y, et al. Mechanistic insights into the thermal deposition of highly thermal-stable jet fuel. Fuel 2020;276(May):118100. http://dx.doi.org/10.1016/j.fuel.2020.118100.
[3] Kuprowicz NJ, Zabarnick S, West ZJ, Ervin JS. Use of measured species class concentrations with chemical kinetic modeling for the prediction of autoxidation and deposition of jet fuels. Energy Fuels 2007;21(2):530–44.
[4] Alborzi E, Blakey S, Ghadbeigi H, Pinna C, Lewis C. Investigation of surface deposition in a simulated fuel injector feed arm with sudden expansion/contraction. Fuel 2016;186:534–43.
[5] Jia T, Zhao M, Pan L, Deng C, Zou J-j, Zhang X. Effect of phenolic antioxidants on the thermal oxidation stability of high-energy-density fuel. Chem Eng Sci 2021;117056. http://dx.doi.org/10.1016/j.ces.2021.117056.
[6] Hazlett RN. Thermal oxidation stability of aviation turbine fuels. Vol. 1. Astm International; 1991.
[7] Mushrush Gw. Fuel instability 1: Organo-sulfur hydroperoxide reactions. Fuel Sci Technol Int 1992;10(9):1523–60. http://dx.doi.org/10.1080/08843759208905361.
[8] Rawson PM, Webster RL, Evans D, Abanteriba S. Contribution of sulfur compounds to deposit formation in jet fuels at 140° C using a quartz crystal microbalance technique. Fuel 2018;231:1–7.
[9] Naegeli DW. The role of sulfur in the thermal stability of jet fuel. In: Turbo expo: Power for land, sea, and air. Vol. 78590. American Society of Mechanical Engineers; 1999, V002T02A053.
[10] Parks CM, Meijer AJ, Blakey SG, Alborzi E, Pourkashanian M. Computational studies on the reactions of thiols, sulfides and disulfides with hydroperoxides. Relevance for jet fuel autoxidation. Fuel 2022;316(January):123326. http://dx.doi.org/10.1016/j.fuel.2022.123326.
[11] van Bergen LA, Roos G, De Proft F. From thiol to sulfonic acid: Modeling the oxidation pathway of protein thiols by hydrogen peroxide. J Phys Chem A 2014;118(31):6078–84.
[12] Beaver B, Gao L, Burgess-Clifford C, Sobkowiak M. On the mechanisms of formation of thermal oxidative deposits in jet fuels. Are unified mechanisms possible for both storage and thermal oxidative deposit formation for middle distillate fuels? Energy Fuels 2005;19(4):1574–9.
[13] Jia T, Zhang X, Liu Y, Gong S, Deng C, Pan L, et al. A comprehensive review of the thermal oxidation stability of jet fuels. Chem Eng Sci 2020;116157.
[14] Mielczarek DC. Autoxidation behaviour of hydrocarbons in the context of conventional and alternative aviation fuels (Ph.D. thesis), (July). University of Leeds; 2015.
[15] Naegeli DW. Thermal stability of jet fuels: Kinetics of forming deposit precursors. Final Report for NASA Contract No. NAG, 1997, p. 3–1739.
[16] Ervin J, Heneghan S, Martel C, Williams T. Surface effects on deposits from jet fuels. In: Turbo expo: Power for land, sea, and air. Vol. 78804. American Society of Mechanical Engineers; 1995, V003T06A017.
[17] Kauffman RE. The effects of different sulfur compounds on jet fuel oxidation and deposition. In: Proceedings of the ASME turbo expo. Vol. 3. 1995, http://dx.doi.org/10.1115/95-GT-222, URL https://proceedings.asmedigitalcollection.asme.org.
[18] Kendall DR, Mills JS. The influence of JFTOT operating parameters on the assessment of fuel thermal stability. SAE Technical Papers, 1985, http://dx.doi.org/10.4271/851871.
[19] Venkataraman R, Eser S. Characterisation of solid deposits from the thermal-oxidative degradation of jet fuel. Int J Oil Gas Coal Technol 2008;1(1–2):126–37.
[20] Raman A, Quiñones R, Barriger L, Eastman R, Parsi A, Gawalt ES. Understanding organic film behavior on alloy and metal oxides. Langmuir 2010;26(3):1747–54.
[21] Mohan AR, Eser S. Analysis of carbonaceous solid deposits from thermal oxidative stressing of Jet-A fuel on iron- and nickel-based alloy surfaces. Ind Eng Chem Res 2010;49(6):2722–30. http://dx.doi.org/10.1021/ie901283r.
[22] Altin O, Eser S. Characterization of carbon deposits from jet fuel on Inconel 600 and Inconel X surfaces. Ind Eng Chem Res 2000;39(3):642–5. http://dx.doi.org/10.1021/ie990694o.
[23] Zabarnick S, Phelps DK. Density functional theory calculations of the energetics and kinetics of jet fuel autoxidation reactions. Energy Fuels 2006;20(2):488–97.
[24] Parks CM, Alborzi E, Blakey SG, Meijer AJ, Pourkashanian M. Density functional theory calculations on copper-mediated peroxide decomposition reactions: Implications for jet fuel autoxidation. Energy Fuels 2020;34(6):7439–47.
[25] Gattinoni C, Ewen JP, Dini D. Adsorption of surfactants on α-Fe2O3 (0001): A density functional theory study. J Phys Chem C 2018;122(36):20817–26.
[26] Sarfo KO, Murkute P, Isgor OB, Zhang Y, Tucker J, Árnadóttir L. Density functional theory study of the initial stages of cl-induced degradation of α-Cr2O3 passive film. J Electrochem Soc 2020;167(12):121508.
[27] Ng M-F, Blackwood DJ, Jin H, Tan TL. DFT study of oxygen reduction reaction on chromia and hematite: Insights into corrosion inhibition. J Phys Chem C 2020;124(25):13799–808.
[28] Cantarelli C, Darenne B, Fortunato MA, de Bruin T, Costa D. DFT screening of adsorption of biodiesel molecules on aluminium and stainless steel surfaces. Results Surf Interfaces 2022;100050.
[29] Kamin R, Ortman M. DoD fuel stability program program drivers. In: CRC conference. No. May. 2019.
[30] Boichenko S, Vovk O, Iakovlieva A. Overview of innovative technologies for aviation fuels production. Publishing House of Lviv Polytechnic National University; 2013.
[31] Evans H, Hilton D, Holm R. Chromium-depleted zones and the oxidation process in stainless steels. Oxidat Met 1976;10(3):149–61.
[32] Rohrbach A, Hafner J, Kresse G. Ab initio study of the (0001) surfaces of hematite and chromia: Influence of strong electronic correlations. Phys Rev B Condens Matter Mater Phys 2004;70(12):1–17. http://dx.doi.org/10.1103/PhysRevB.70.125426.
[33] Guo H, Barnard AS. Thermodynamic modelling of nanomorphologies of hematite and goethite. J Mater Chem 2011;21(31):11566–77.
[34] Kopač D, Jurković DL, Likozar B, Huš M. First-principles-based multiscale modelling of nonoxidative butane dehydrogenation on Cr2O3 (0001). ACS Catal 2020;10(24):14732–46.
[35] Ovcharenko R, Voloshina E, Sauer J. Water adsorption and O-defect formation on Fe2O3(0001) surfaces. Phys Chem Chem Phys 2016;18(36):25560–8. http://dx.doi.org/10.1039/c6cp05313k.
[36] Wang XG, Smith JR. Surface phase diagram for Cr2O3(0001): Ab initio density functional study. Phys Rev B Condens Matter Mater Phys 2003;68(20):3–6. http://dx.doi.org/10.1103/PhysRevB.68.201402.
[37] Hill A, Jiao F, Bruce P, Harrison A, Kockelmann W, Ritter C. Neutron diffraction study of mesoporous and bulk hematite, α-Fe2O3. Chem Mater 2008;20(15):4891–9.

[38] Golosova N, Kozlenko D, Kichanov S, Lukin E, Liermann H-P, Glazyrin K, et al. Structural and magnetic properties of Cr2O3 at high pressure. J Alloys Compd 2017;722:593–8.
[39] Jain A, Hautier G, Moore CJ, Ong SP, Fischer CC, Mueller T, et al. A high-throughput infrastructure for density functional theory calculations. Comput Mater Sci 2011;50(8):2295–310.
[40] Kamrani Moghaddam L, Ramezani Paschepari S, Zaimy MA, Abdalaian A, Jebali A. The inhibition of epidermal growth factor receptor signaling by hexagonal selenium nanoparticles modified by SiRNA. Cancer Gene Ther 2016;23(9):321–5. http://dx.doi.org/10.1038/cgt.2016.38.
[41] Kresse G, Hafner J. Ab initio molecular dynamics for liquid metals. Phys Rev B 1993;47(1):558.
[42] Kresse G, Furthmüller J. Efficiency of ab-initio total energy calculations for metals and semiconductors using a plane-wave basis set. Comput Mater Sci 1996;6(1):15–50.
[43] Kresse G, Furthmüller J. Efficient iterative schemes for ab initio total-energy calculations using a plane-wave basis set. Phys Rev B 1996;54:11169–86. http://dx.doi.org/10.1103/PhysRevB.54.11169, URL https://link.aps.org/doi/10.1103/PhysRevB.54.11169.
[44] Román-Pérez G, Soler JM. Efficient implementation of a van der waals density functional: Application to double-wall carbon nanotubes. Phys Rev Lett 2009;103:096102. http://dx.doi.org/10.1103/PhysRevLett.103.096102, URL https://link.aps.org/doi/10.1103/PhysRevLett.103.096102.
[45] Raman A, Gawalt ES. Self-assembled monolayers of alkanoic acids on the native oxide surface of SS316L by solution deposition. Langmuir 2007;23(5):2284–8.
[46] Therrien AJ, Hensley AJ, Hannagan RT, Schilling AC, Marcinkowski MD, Larson AM, et al. Surface-templated assembly of molecular methanol on the thin film '29' Cu (111) surface oxide. J Phys Chem C 2019;123(5):2911–21.
[47] Murphy CJ, Carrasco J, Lawton TJ, Liriano ML, Baber AE, Lewis EA, et al. Structure and energetics of hydrogen-bonded networks of methanol on close packed transition metal surfaces. J Chem Phys 2014;141(1):014701.
[48] Vericat C, Vela ME, Corthey G, Pensa E, Cortés E, Fonticelli MH, et al. Self-assembled monolayers of thiolates on metals: A review article on sulfur-metal chemistry and surface structures. Rsc Adv 2014;4(53):27730–54.
[49] Noh J, Kato HS, Kawai M, Hara M. Surface and adsorption structures of dialkyl sulfide self-assembled monolayers on Au (111). J Phys Chem B 2002;106(51):13268–72.
[50] Kresse G, Joubert D. From ultrasoft pseudopotentials to the projector augmented-wave method. Phys Rev B 1999;59(3):1758.
[51] Blöchl PE. Projector augmented-wave method. Phys Rev B 1994;50(24):17953.
[52] Tang W, Sanville E, Henkelman G. A grid-based Bader analysis algorithm without lattice bias. J Phys: Condens Matter 2009;21(8):084204.
[53] Sanville E, Kenny SD, Smith R, Henkelman G. Improved grid-based algorithm for Bader charge allocation. J Comput Chem 2007;28(5):899–908.
[54] Henkelman G, Arnaldsson A, Jónsson H. A fast and robust algorithm for Bader decomposition of charge density. Comput Mater Sci 2006;36(3):354–60.
[55] Yu M, Trinkle DR. Accurate and efficient algorithm for Bader charge integration. J Chem Phys 2011;134(6):064111.
[56] Bartók AP, Yates JR. Regularized SCAN functional. J Chem Phys 2019;150(16):161101.
[57] Sun J, Stirner T, Matthews A. Structure and surface energy of low-index surfaces of stoichiometric α-Al2O3 and α-Cr2O3. Surf Coat Technol 2006;201(7):4205–8.
[58] Wang X-G, Weiss W, Shaikhutdinov SK, Ritter M, Petersen M, Wagner F, et al. The hematite (α-Fe 2 O 3)(0001) surface: evidence for domains of distinct chemistry. Phys Rev Lett 1998;81(5):1038.
[59] Antonio EN, Wicking C, Filip S, Ryan MP, Heutz S. Role of iron speciation in oxidation and deposition at the hexadecane-iron interface. ACS Appl Mater Interf 2020. http://dx.doi.org/10.1021/acsami.9b22983.
[60] Eser S, Venkataraman R, Altin O. Deposition of carbonaceous solids on different substrates from thermal stressing of JP-8 and jet A fuels. Ind Eng Chem Res 2006;45(26):8946–55. http://dx.doi.org/10.1021/ie060968p.
[61] Balster LM, Zabarnick S, Striebich RC, Shafer LM, West ZJ. Analysis of polar species in jet fuel and determination of their role in autoxidative deposit formation. Energy Fuels 2006;20(6):2564–71.
[62] Gadsby P. Surface roughness effects on thermally stressed aviation fuel. 2018, URL http://etheses.whiterose.ac.uk/19191/1/Thesis-Pichilemu.pdf.
[63] Duangthip T, Ervin JS. Simulations of jet fuel thermal oxidative degradation: Part I. The effect of metal surface catalysis on the thermal oxidation of jet fuel. Tech. rep., 2006, URL https://www.me.psu.ac.th/ME_NETT20/article/pdf/tsf/TSF039.pdf.
[64] Alborzi E, Blakey S, Ghadbeigi H, Pinna C. Prediction of growth of jet fuel autoxidative deposits at inner surface of a replicated jet engine burner feed arm. Fuel 2018;214:528–37. http://dx.doi.org/10.1016/j.fuel.2017.10.006, URL https://www.sciencedirect.com/science/article/pii/S0016236117312528.
[65] Alborzi E, Dwyer MR, Parks CM, Sheikhansari A, Mielczarek DC, Zanganeh M, et al. Construction of a reduced chemical kinetic mechanism for autoxidation of n-paraffinic solvent - A model for aviation fuel. Fuel 2021;294(January):120170. http://dx.doi.org/10.1016/j.fuel.2021.120170.
[66] Mamun O, Winther KT, Boes JR, Bligaard T. High-throughput calculations of catalytic properties of bimetallic alloy surfaces. Sci Data 2019;6(1):1–9. http://dx.doi.org/10.1038/s41597-019-0080-z.